Astron. Astrophys. 356, 1010–1022 (2000)

ASTRONOMY AND ASTROPHYSICS

The ortho:para-H_2 ratio in C- and J-type shocks⋆

D. Wilgenbus[1], **S. Cabrit**[1], **G. Pineau des Forêts**[2,3], **and D.R. Flower**[4]

[1] Observatoire de Paris, DEMIRM, UMR 8540 du CNRS, 61 Avenue de l'Observatoire, 75014 Paris, France
[2] Observatoire de Paris, DAEC, UMR 8631 du CNRS, 92195 Meudon Principal Cedex, France
[3] Université Paris XI, Institut d'Astrophysique Spatiale, 91405 Orsay Cedex, France
[4] The University, Physics Department, Durham DH1 3LE, UK

Received 16 November 1999 / Accepted 8 February 2000

Abstract. We have computed extensive grids of models of both C- and J-type planar shock waves, propagating in dark, cold molecular clouds, in order to study systematically the behaviour of the ortho:para-H_2 ratio. Careful attention was paid to both macroscopic (dynamical) and microscopic (chemical reactions and collisional population transfer in H_2) aspects. We relate the predictions of the models to observational determinations of the ortho:para-H_2 ratio using both pure rotational lines and rovibrational lines. As an illustration, we consider ISO and ground-based H_2 observations of HH 54. Neither planar C-type nor planar J-type shocks appear able to account fully for these observations. Given the additional constraints provided by the observed ortho:para H_2 ratios, a C-type bowshock, or a C-type precursor followed by a J-type shock, remain as plausible models.

Key words: Magnetohydrodynamics (MHD) – molecular processes – shock waves – ISM: individual objects: HH 54 – ISM: molecules – infrared: ISM: lines and bands

1. Introduction

Interest in emission by molecular hydrogen and, more specifically, in the ortho:para-H_2 ratio has been stimulated by observations of the pure rotational lines of H_2 made with the ISO satellite. Ortho:para ratios ≈ 1 have been determined from ISO observations of these lines towards several regions associated with outflows from young stellar objects, such as HH 54 (Neufeld et al. 1998; Cabrit et al. 1999), in which shocks are believed to be propagating.

The evolution of the ortho:para-H_2 ratio in interstellar gas was studied by Osterbrock (1962), Dalgarno et al. (1973), DeCampli et al. (1978), Clavel et al. (1978), Flower & Watt (1984), Pineau des Forêts et al. (1991), and recently by Timmermann (1998). It is known that this ratio can be modified by reactive collisions with protons or proton-transferring ions, such as H_3^+. Whilst reactions with protons do not exhibit a significant activation energy (Gerlich 1990), the barrier to hydrogen atom reactions is approximately 5000 K (Siegbahn & Liu 1978). It follows that reactive collisions with hydrogen atoms are significant only in hot gas, notably in gas which has been heated by the passage of a shock wave. Furthermore, as shown by Flower & Watt (1984), the timescale for the ortho:para ratio to subsequently equilibrate in the cold gas can exceed 10^6 yr. In regions of low-mass star formation, gas which has undergone shock heating in an episodic event is unlikely to return to equilibrium between such events, given their estimated frequency, of the order of 10^{-3} yr^{-1} (see, for example, Devine et al. 1997).

Timmermann (1998) studied the variation of the ortho:para-H_2 ratio through C-type shock waves propagating in predominantly molecular gas. Shock speeds $10 < V_{\rm s} < 30$ km s^{-1} and preshock densities $10^2 < n_{\rm H} < 10^6$ cm^{-3} were considered. Crucial to a correct evaluation of the ortho:para ratio are the fraction of atomic hydrogen, the temperature of the neutrals, the degree of ionization, and the ion-neutral drift speed. An adequate description of the cooling of the gas, particularly by H_2, and of its chemistry are indispensable to the reliable prediction of these parameters. In the present paper, we re-examine the problem of ortho:para conversion in C-type shocks. Our models include a more accurate treatment of the above phenomena and make use of recent calculations of rate coefficients for the collisional excitation of H_2. As will be seen below, the results of our calculations differ substantially from those of Timmermann (1998) in a number of significant respects. For the purposes of comparison, we have also investigated H_2 emission and ortho:para conversion in non-dissociative J-type shocks.

In Sect. 2, the theory relating to the models that we have used is summarized. Our results, for both C- and J-type shocks, are described and discussed in Sect. 3. In Sect. 4, we discuss diagnostics available for constraining the initial ortho:para ratio in shocks, and we consider briefly the interpretation of ISO observations of HH 54, postponing a more extensive treatment of this and other sources to a subsequent paper.

2. Theoretical models

We consider both C- and J-type shocks. The equations for the H_2 rovibrational level populations are integrated in parallel with

Send offprint requests to: david.wilgenbus@obspm.fr

⋆ Tables 2a-f and 4a-f are only available in electronic form at the CDS via anonymous ftp to cdsarc.u-strasbg.fr (130.79.128.5) or via http://cdsweb.u-strasbg.fr/Abstract.html

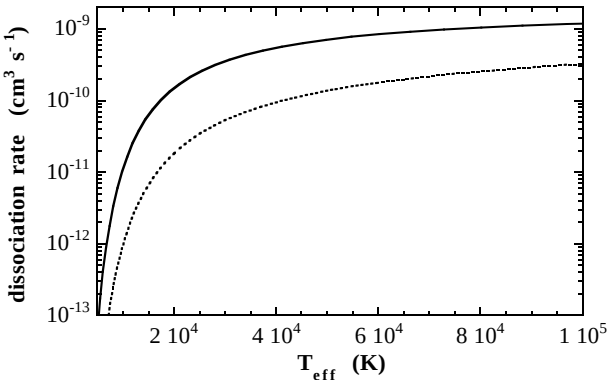

Fig. 1. Rate coefficient (in cm^3 s^{-1}) for the collisional dissociation of H_2 by heavy ion impact. Full curve: Langevin model (Draine et al. 1983); broken curve: assuming a constant cross section; see text, Sect. 2.1.

the hydrodynamic equations (Flower & Pineau des Forêts 1999), as in the studies of Timmermann (1998) and Chang & Martin (1991). We take advantage of the more complete and reliable data that now exist for the collisional excitation of H_2 by H, He, and H_2 (Le Bourlot et al. 1999), including the 49 rovibrational levels of H_2 with energies up to 20 000 K. The treatment of ortho:para interconversion was adopted from Le Bourlot et al. (1999). We pay careful attention to the chemistry of the gas, particularly the ion chemistry, incorporating a total of 120 species and a network of 864 reactions (see Schilke et al. 1997 and references therein). The MHD and chemical rate equations are solved in parallel in order to allow correctly for the effects of changes in the degree of ionization on the structure of the shock wave: see Sect. 2.2. The drag on the neutral fluid owing to collisions with charged grains is also included, adopting a standard gas to dust ratio and grain size distribution (Mathis et al. 1977).

Our treatment of the thermal balance of the gas includes the contributions to the cooling of species other than H_2 (the only coolant considered by Chang & Martin), namely C, O, C^+, H_2O, CO, OH, and NH_3. More detailed information on the models may be found in the papers of Flower & Pineau des Forêts (1999), Chièze et al. (1998), Schilke et al. (1997), and Flower et al. (1996).

2.1. Collisional dissociation of H_2

Dissociation of H_2 by electron impact, which proceeds mainly via the $b^3\Sigma_u^+$ state of H_2 (Stibbe & Tennyson 1998), and by H atom impact (Dove & Mandy 1986) have been taken into account. The rate of collisional dissociation of H_2 by H_2 impact, under the low-density conditions prevailing in the interstellar medium, is poorly known. Measurements in shock tubes (Jacobs et al. 1967; Breshears & Bird 1973) yielded a rate coefficient for dissociation of H_2 by H_2 which is approximately an order of magnitude smaller than in H_2 - H collisions. However, the densities in laboratory shock tubes are vastly greater than in the interstellar gas, and the relevance of such measurements to interstellar conditions, where only the few lowest rotational states are significantly populated, has been questioned by Dove & Mandy (1986). Ultimately, we decided to include dissociation in H_2 - H_2 collisions, with a rate coefficient 8 times smaller than for H - H_2, as indicated by the shock tube measurements; but we recognize that this may yield an overestimate of the contribution of this process.

Not included in our previous studies, but incorporated here, is the collisional dissociation of H_2 by ion impact. Timmermann (1998) allowed for dissociation of H_2 by a representative non-reactive positive ion I^+ of mass $32m_{\rm H}$, adopting the rate coefficient for collisional dissociation from Draine et al. (1983). These authors allowed for the thermal contribution and, more important in practice, that of ion-neutral drift, to this process. For the range of drift speeds of interest here, the rate coefficient of Draine et al. is well reproduced by the functional form (shown as a solid line in Fig. 1)

$$\langle\sigma v\rangle\,{\rm cm^3 s^{-1}} = 2\times10^{-9}\exp(-52000/T_{\rm eff}) \qquad (1)$$

where

$$T_{\rm eff} = (m_{\rm i}T_{\rm n}+m_{\rm n}T_{\rm i})/(m_{\rm i}+m_{\rm n}) + m_{\rm in}(V_{\rm i}-V_{\rm n})^2/(3k_{\rm B}) \qquad (2)$$

and m is a mass, T a kinetic temperature, V a flow velocity, $k_{\rm B}$ is Boltzmann's constant, and 'i' refers to an ion, 'n' to a neutral (in practice, H_2); the reduced mass, $m_{\rm in} = m_{\rm i}m_{\rm n}/(m_{\rm i}+m_{\rm n})$. Note that, for a heavy molecular ion with $m_{\rm i} \gg m_{\rm n}$, $m_{\rm in} \simeq m_{\rm n} = 2m_{\rm H}$, and the first term on the rhs of Eq. (2) is approximately equal to $T_{\rm n}$.

We shall see below that, even when we include collisional dissociation of H_2 by I^+, with the above rate coefficient, our results differ from those of Timmermann (1998). Specifically, the degree of dissociation of the gas (fraction of atomic hydrogen) which we obtain is less than Timmermann predicted, with important consequences for the ortho:para-H_2 ratio.

Draine et al. (1983) derived the rate coefficient for dissociation of H_2 by ion impact using the Langevin ('orbiting') model of ion-neutral collisions, assuming that dissociation occurs following each orbiting collision; this procedure yields an upper bound to the actual rate of dissociation. The orbiting model is appropriate at low collision energies, comparable with the well depth of the ion-neutral interaction, which is unlikely to exceed 0.1 eV. However, at collision velocities > 10 km s^{-1}, required for the rate of dissociation by ion impact to become significant, the collision energy > 1 eV, and the orbiting model is inappropriate. We believe that a better approximation to the rate coefficient at these high energies may be obtained by assuming a constant cross section, $\sigma = \pi a^2$, where a has been taken equal to the H_2 internuclear distance ($a = 0.74\times10^{-8}$ cm), whence

$$\langle\sigma v\rangle\,{\rm cm^3 s^{-1}} = 3\times10^{-11}\sqrt{\frac{T_{\rm eff}}{300}}\,\exp(-52000/T_{\rm eff}) \qquad (3)$$

where 52 000 K is the dissociation energy of H_2 (4.48 eV), expressed in K through division by $k_{\rm B}$. The rate coefficient which derives from Eq. (3) is plotted in Fig. 1 as a dashed line. As expected, it lies below the prediction of the orbiting model.

Table 1. Initial values of the densities (cm^{-3}) of the listed species as calculated here, in equilibrium, for $n_H = 10^3$, 10^4, 10^5, and 10^6 cm^{-3}, and as given by Timmermann (1998) for $n_H = 10^4$ cm^{-3}. Timmermann adopted an initial gas kinetic temperature T = 35 K and cosmic ray ionization rate $\zeta = 2\times10^{-17}$ s^{-1}; we chose T = 10 K and $\zeta = 5\times10^{-17}$ s^{-1}. Numbers in parentheses are powers of 10.

Species	Equilibrium				Timmermann (1998)
n_H	1.00(3)	1.00(4)	1.00(5)	1.00(6)	1.00(4)
H_2	4.99(2)	5.00(3)	5.00(4)	4.99(5)	5.00(3)
H	2.95(0)	3.68(0)	5.15(0)	5.29(0)	1.00(1)
CO	1.41(-1)	1.41(0)	1.41(1)	1.41(2)	4.00(-1)
C	4.86(-4)	3.88(-4)	3.12(-4)	2.53(-4)	5.00(-1)
C^+	6.05(-6)	5.11(-6)	4.68(-6)	5.51(-6)	1.00(-3)
O	3.65(-1)	3.32(0)	3.15(1)	3.08(2)	4.25(0)
H_2O	9.35(-3)	7.59(-2)	4.81(-1)	3.13(0)	1.00(-2)
H^+	9.35(-6)	8.97(-6)	9.81(-6)	1.02(-5)	2.00(-4)
H_3^+	2.82(-5)	3.50(-5)	3.81(-5)	3.96(-5)	2.00(-5)
I^+					1.00(-3)
S^+	2.59(-4)	3.96(-4)	5.80(-4)	9.29(-4)	
n_i	3.53(-4)	6.60(-4)	1.47(-3)	5.32(-3)	2.22(-3)

Of course, the correct rate of dissociation by ion impact could prove to be even smaller than this revised estimate.

2.2. Initial conditions and chemistry

As we wish to study ortho:para H_2 conversion in shocks, starting from values < 3, we shall consider a cold molecular cloud shielded from the external UV field ($A_v > 5$ mag), as appropriate for regions of moderate star formation efficiency located away from photodissociation fronts. In Table 1, we list the initial species densities that we calculate, in equilibrium, for n_H= 10^3, 10^4, 10^5, and 10^6 cm^{-3}, assuming T = 10 K and a cosmic ray ionization rate $\zeta = 5\times10^{-17}$ s^{-1}. For comparison, we also list the initial species densities adopted by Timmermann (1998; Table 1, model 2) for n_H = 10^4 cm^{-3}. There are surprisingly large differences, between our initial values and those of Timmermann, for some of the species listed in Table 1, particularly C, C^+, and H^+. These differences are not attributable to the different cosmic ray ionization rates and initial temperatures. I^+ is the non-reactive ion of mass $32m_H$, introduced by Timmermann. S^+ has the same mass, and its equilibrium abundance is also given in Table 1. Note that S^+ is reactive in the shock wave, where a sequence of hydrogen abstractions is initiated by the endothermic reaction $S^+(H_2, H)SH^+$, which is driven by ion-neutral streaming. The abundances of other ions, such as H_3^+ and H^+, also tend to decrease, owing to the compression of the gas by the shock wave. This compression enhances the rates of reactions such as $H_3^+(O, H_2)OH^+$ and leads ultimately to a decrease in the fractional ionization of the gas, through dissociative recombination of the molecular ions with electrons. Also important are the reactions $O(H_2, H)OH$ and $OH(H_2, H)H_2O$, which produce two hydrogen atoms for each oxygen atom removed. These reactions have activation energies, which can be thermally surmounted in the shock-heated gas. As we shall see below, they are important contributors of atomic hydrogen and thence influence the variation of the ortho:para-H_2 ratio through the shock wave.

As can be judged from Table 1, the equilibrium values of both the ion and atomic hydrogen densities are initially low under the dense dark cloud conditions considered here. As the (proton-transferring) ions and H atoms modify the ortho:para-H_2 ratio in the shock wave, the timescale for this process to occur may be comparable with the duration of the shock pulse. Under these circumstances, the initial value of the ortho:para ratio is significant in determining the integral value of this parameter. In view of this fact, the initial value of the ortho:para ratio has been taken to be a free parameter of the model. The time required for this ratio to reach equilibrium in gas of density n_H= 10^4 cm^{-3}, in which $n(H^+) + n(H_3^+) \simeq 10^{-4}$ cm^{-3}, approaches 10^6 yr. If the gas is cold, the equilibrium ortho:para ratio is small (< 0.01 at $T < 25$ K). Passage through a shock wave with a maximum temperature exceeding about 500 K will, as we shall see below, cause this ratio to increase rapidly to a value of the order of 1, and a further 10^5 - 10^6 yr are then required for the ratio to relax to its equilibrium value in the postshock gas. We may therefore conclude that, if a low ($\ll 1$) initial value of the ortho:para ratio is implied by observation, e.g. of an outflow source, then the gas is unlikely to have been significantly heated by the shock wave associated with an earlier outflow in the same jet, given that the time between such episodes is believed to be much less than that required for the ortho:para ratio to return to equilibrium. In the present calculations, we consider initial ortho:para ratios between 0.01 and 3.0.

3. Results and discussion

3.1. C-type shocks

3.1.1. Comparison with Timmermann (1998)

Timmermann (1998) presented profiles for 3 models of C-type shocks with speed V_s= 20 km s^{-1} and initial densities n_H= $10^2, 10^4$ and 10^6 cm^{-3}. In Fig. 2, we compare his and our corresponding results in the case of n_H= 10^4 cm^{-3}, for which the initial magnetic induction B = 100 μG; the initial ortho:para ratio is 1. Collisional dissociation of H_2 by a non-reactive ion I^+ of mass $32m_H$ was included in both calculations, adopting the rate coefficient of Draine et al. (1983) (see Sect. 2.1).

Whilst the shock widths and temperature profiles are similar in the two calculations shown in Fig. 2, important differences also emerge. The increase in the atomic hydrogen density, owing to dissociation of H_2 in the shock wave, is much smaller in our model than in that of Timmermann and, consequently, the maximum ortho:para ratio that is attained is also less. The behaviour of the ion (H^+, H_3^+) densities is very different. Timmermann's calculation shows an initial rise in $n(H^+)$ and $n(H_3^+)$, presumably due to the compression of the ionized fluid, which precedes that of the neutrals. In our model, this rise is quenched, even reversed, by chemical reactions which remove ions, as discussed in Sect. 2 above. The total density of ions in our shock model is only 10^{-3} cm^{-3}, an order of magnitude smaller than the H_3^+

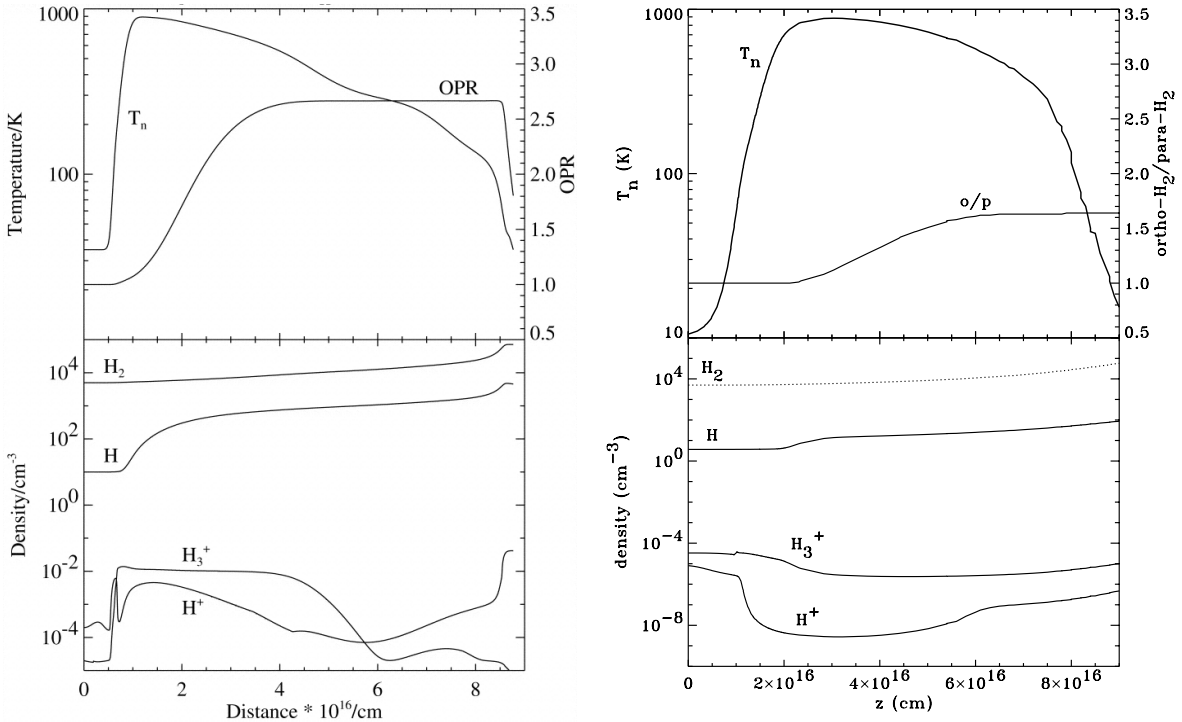

Fig. 2. A comparison of the shock profiles of (left) Timmermann (1998, model 2) and (right) ourselves, using the same rate coefficient for dissociation by a non-reactive ion I^+ of mass $32m_{\rm H}$. The temperature of the neutral fluid and the ortho:para-H_2 ratio are plotted in the upper panels, the densities of selected species in the lower panels.

density alone in Timmermann's model. Perhaps the most puzzling aspect of Timmermann's results is the rapid rise in the density of H^+ as the gas cools towards its postshock temperature; this increase coincides with the compression of the neutrals. We know of no reason for such an increase in the H^+ density: cosmic ray ionization occurs on a distance scale which is orders of magnitude larger. We tentatively conclude that the treatment, in Timmermann's model, of the chemistry of these ions is incomplete or incorrect. The higher ion abundance, calculated by Timmermann, has direct and indirect (through the rate of formation of H by ion impact dissociation of H_2) consequences for the ortho:para ratio; the net effect is an overestimation of the ortho:para ratio in Timmermann's calculations.

3.1.2. A grid of models

In what follows, we continue to include the dissociation of H_2 by ions, but only real and chemically active ions are considered and the rate coefficient is derived assuming a constant cross section, as described in Sect. 2. Models of C-type shocks were calculated for

- initial densities $n_{\rm H}$= n(H) + 2n(H_2) = 10^3, 10^4, 10^5, 10^6 cm^{-3},
- initial ortho:para ratios (o/p)$_{\rm init}$ = 0.01,1.0, 2.0, 3.0,
- shock speeds $V_{\rm s}$= 10, 20, 30, 40 km s^{-1}(except for $n_{\rm H}$= 10^6 cm^{-3}, when $V_{\rm s}$= 10, 15, 20, 25, 30 km s^{-1}).

We obtain the initial magnetic induction from $B(\mu{\rm G}) = [n_{\rm H}({\rm cm}^{-3})]^{1/2}$.

The left-hand column of Fig. 3 shows the variations of the temperature of the neutrals, $T_{\rm n}$, of the fractional abundance of H, n(H)/$n_{\rm H}$, and of the local ortho:para ratio, n(ortho)/n(para), through C-type shock waves with $10 < V_{\rm s} < 40$ km s^{-1}, and, initially, $n_{\rm H}$= 10^4 cm^{-3} and ortho:para = 0.01. We note that allowance for the chemical reactivity of the ions has important consequences, notably for the width of the shock wave (see Pineau des Forêts et al. 1997). The reduction in the density of ions, owing to their removal in chemical reactions, results in a wider shock wave; the increase in width is a factor of 2 for $n_{\rm H}$= 10^4 cm^{-3} and $V_{\rm s}$= 20 km s^{-1} (compare Fig. 3a with right panel of Fig. 2).

Fig. 3d compares, for $n_{\rm H}$= 10^4 cm^{-3} and $V_{\rm s}$= 40 km s^{-1}, the rates (in s^{-1}) of the various processes which contribute to the dissociation of H_2: collisional dissociation by electrons, by hydrogen atoms and molecules, and by ions; chemical dissociation, including neutral-neutral reactions of the type O(H_2, H)OH, OH(H_2, H)H_2O. At this high shock (and hence ion-neutral drift) speed, the rate of dissociation by ion impact exceeds the rate of production of H by chemical conversion of oxygen into water. The dissociation rate is of the order of 10^{-13} s^{-1} over much of the shock width. Estimating the flow time of the neutrals through the shock wave as 10^{17} cm/3 $\times$ 10^6 cm s^{-1} $\approx 3\times10^{10}$ s, the fraction of H_2 that is dissociated is given approximately by 3×10^{10} s/ 10^{13} s = 3×10^{-3}; this estimate is confirmed by the numerical results (Fig. 3b). At a lower shock speed, $V_{\rm s}$= 20 km s^{-1}, collisional dissociation by ions becomes insignificant, and neutral-neutral reactions initiated by O turn

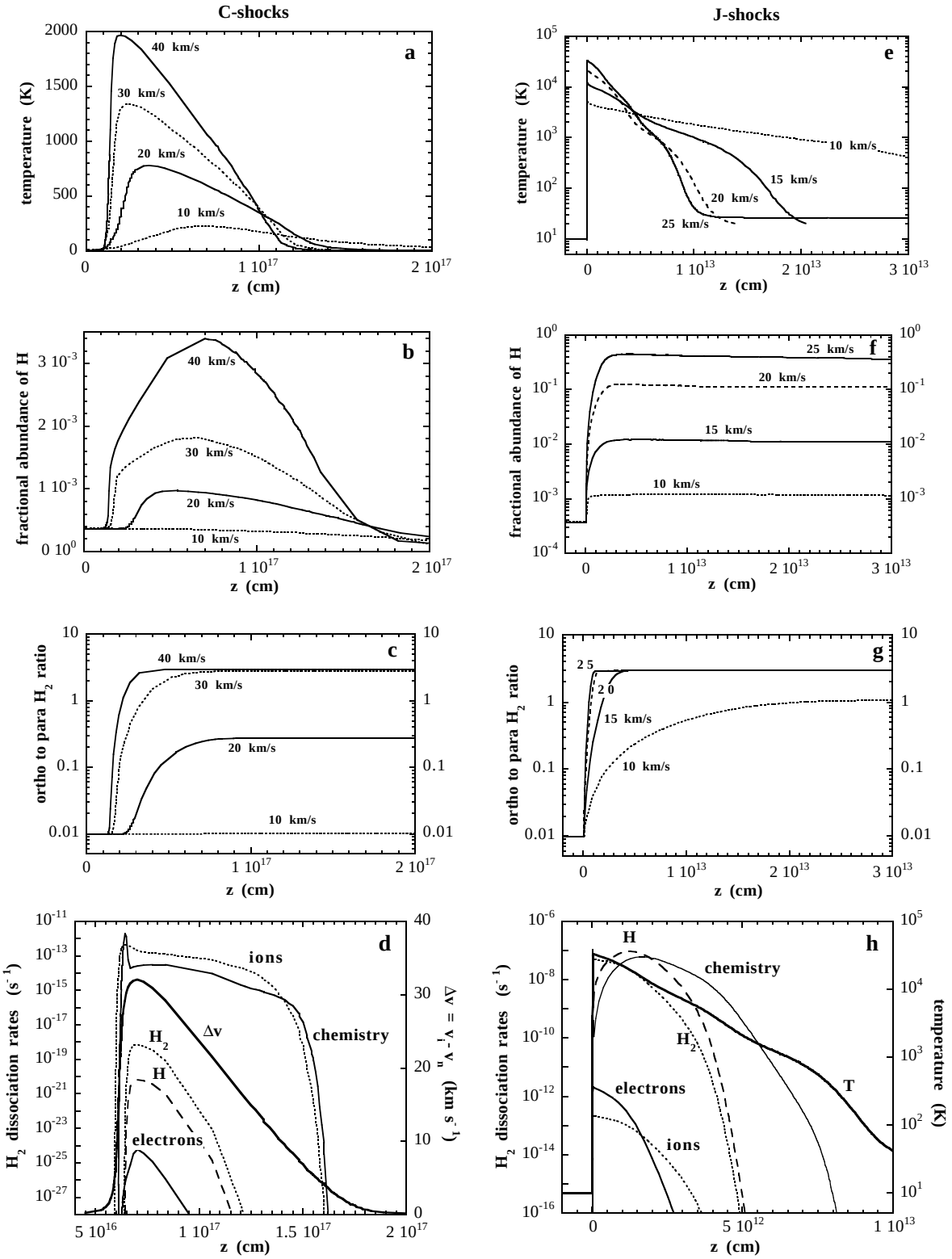

Fig. 3a–h. The variation of (**a**) the temperature of the neutrals, $T_{\rm n}$(K), (**b**) the fractional abundance of H, $n(H)/n_{\rm H}$, and (**c**) the ortho:para ratio through C-type shock waves with $10 < V_{\rm s} < 40$ km s^{-1}; initially, $n_{\rm H} = 10^4$ cm^{-3}, B = 100 μG, and the ortho:para ratio is 0.01. (**d**) The rates (s^{-1}) of the processes which contribute to the dissociation of H_2, and production of H, in a C-type shock with $V_{\rm s} = 40$ km s^{-1}, and, initially, $n_{\rm H} = 10^4$ cm^{-3} and B = 100 μG. (**e**) Temperature profiles, (**f**) fractional abundance of H, n(H)/$n_{\rm H}$, and (**g**) n(ortho)/n(para) for J-type shocks with speeds $10 < V_{\rm s} < 25$ km s^{-1}; the initial gas density is $n_{\rm H} = 10^4$ cm^{-3}, the initial ortho:para ratio is 0.01, and B = 10 μG. (**h**) The rates (s^{-1}) of the processes which contribute to the dissociation of H_2, and production of H, in a J-type shock in which $V_{\rm s} = 25$ km s^{-1}, and, initially, $n_{\rm H} = 10^4$ cm^{-3} and B = 10 μG.

out to be the most important; the resulting fraction of atomic H is of order 10^{-3}. For V_s= 10 km s^{-1}, the temperature remains too low to activate these reactions and the atomic H fraction does not increase from its initial (preshock) value of 3.7×10^{-4} (Table 1).

3.1.3. Conversion of para- to ortho-H_2

The activation energy of approximately 5000 K for the reaction of H with H_2 makes the efficiency of para to ortho conversion strongly dependent on the maximum neutral temperature reached in the shock wave, $T_{\rm n}^{\rm max}$. As shown in Fig. 3c, for $n_{\rm H}$= 10^4 cm^{-3}, conversion is negligible for $V_{\rm s}$= 10 km s^{-1}($T_{\rm n}^{\rm max}$= 200 K), only partial at 20 km s^{-1}($T_{\rm n}^{\rm max}$= 700 K), and complete for $V_s \geq 30$ km s^{-1}($T_{\rm n}^{\rm max} \geq$ 1300 K). We have found that these threshold temperatures (700 K to start conversion, and 1300 K to reach the statistical value of 3) are valid across the whole grid of models, irrespective of the initial values of the ortho:para ratio and $n_{\rm H}$.

The weak dependence on $n_{\rm H}$ can be understood as follows. The number of para to ortho conversion per H_2 molecule across the shock is given by the integral of $n({\rm H})k(T)dt$ over the shock profile, where $k(T)$ is the reaction rate coefficient at temperature T (averaged over all H_2 levels). We have seen that, even allowing for the contribution of collisional dissociation by ions, the fraction of atomic H in C-type shocks remains always close to 10^{-3} (Fig. 3b). Since $n_{\rm H}$ is approximately constant on the hot plateau, where conversion takes place, n(H) can be considered to be roughly proportional to $n_{\rm H}$ for all the models. The flow time, on the other hand, is found to be inversely proportional to $n_{\rm H}$ (see Table 2). The dependence on $n_{\rm H}$ cancels, leaving $T_{\rm n}^{\rm max}$ as the main parameter controlling para to ortho conversion in our models. The weak dependence on (o/p)$_{\rm init}$ is due to the sudden onset of conversion, once the temperature is sufficiently close to the reaction barrier.

3.1.4. Electronic tables

We provide in Table 2a-f (electronic form only, available at `CDS` and from `http://ccp7.dur.ac.uk/`) an extensive set of parameters, derived from our grid of C-type shock models. Table 3 contains a subset of the results in Table 2a-b, by way of illustration, for $n_{\rm H}$= 10^4 cm^{-3} and (o/p)$_{\rm init}$ = 0.01 and 1.

Table 2a lists for each model: the shock width L (of the region in which $T_{\rm n}>$ 50 K); flow time t (time required for the neutral fluid to traverse the width of the shock wave); n(H)(50 K) (postshock density at $T_{\rm n}$= 50 K); $|v_i - v_n|_{\rm max}$ (maximum ion-neutral drift velocity in the shock wave); $[n({\rm H})/n_{\rm H}]_{\rm max}$; $T_{\rm n}^{\rm max}$ (maximum temperature of the neutrals); $\langle T_J \rangle$ (mean of the excitation temperature T_J, defined by Eq. 6, for levels $v = 0, J = 5$ to 8); $\langle T_J \rangle_{\rm v=1}$ (mean of the excitation temperature T_J, defined by Eq. 6, for levels $v = 1, J = 1$ to 11); n(ortho)/n(para) and N(ortho)/N(para) at the rear of the shock wave (where $T_{\rm n}$ has fallen to 50 K); $(o/p)_{\rm CAM}$ (mean of the empirical ortho:para ratio, derived from Eq. 5, for levels $v = 0, J = 5$ to 8); $(o/p)_{\rm v=1}$ (mean of the empirical ortho:para ratio, derived from Eq. 5, for levels $v = 1, J = 1$ to 11).

Table 2b lists for each model: the initial mechanical energy flux, $\rho V_s^3/2$ (in erg cm^{-2} s^{-1}); $\varepsilon_{\rm H_2}$ (percentage of the initial mechanical energy flux radiated in all the lines of H_2 included in the model); $\varepsilon_{\rm CAM}$ (percentage of the initial mechanical energy flux radiated in the transitions 0-0 S(2) to S(7)); flux radiated in each of the H_2 lines: 0-0 S(0) to S(11); 1-0 S(0) to S(11); and 2-1 S(1) (in erg cm^{-2} s^{-1} sr^{-1}).

Table 2c contains, for all of our models with $n_{\rm H}$= 10^3 cm^{-3}, the column densities of each of the 49 levels of H_2, divided by their statistical weights and sorted by increasing energy $E_J/k_{\rm B}$ above the ground level.

Tables 2d,e,f are the same as Table 2c but for $n_{\rm H}$= 10^4, 10^5, and 10^6 cm^{-3}.

3.2. J-type shocks

It is well known that C-type shocks occur only if the transverse magnetic field strength in the preshock gas exceeds a critical value (cf. Draine 1980). In practice, the magnetic field strength in specific objects is often unknown and must be derived from energy-equipartition arguments, which lead to density-scaling relations of the type used above. However, even if the initial magnetic field strength is sufficiently high for a C-type shock wave to obtain in steady-state, time-dependent calculations (Chièze et al. 1998) show that an initially J-type shock evolves through a mixed C- and J-type structure to ultimately become C-type. Furthermore, the time of evolution to steady state can be comparable with or exceed the estimated lifetimes of molecular outflows. Given the uncertainty in the initial value of the transverse component of the magnetic induction, and the fact that the shock will have a J-type component at early times, we have additionally studied the variation of the ortho:para-H_2 ratio in J-type shocks.

3.2.1. Shock structure and H_2 emission

A grid of J-type shock models was computed for

- $n_{\rm H}$= 10^3, 10^4, 10^5, 10^6 cm^{-3},
- (o/p)$_{\rm init}$ = 0.01, 1.0, 2.0, 3.0,
- $V_{\rm s}$= 5, 10, 15, 20, 25 km s^{-1}.

A small but finite initial magnetic induction was assumed, $B(\mu{\rm G})$ = 0.1$[n_{\rm H}({\rm cm}^{-3})]^{1/2}$, which is an order of magnitude smaller than adopted in Sect. 3.1 above for the same initial gas density. The other initial conditions were the same as in the corresponding C-type shock model. When computing the J-type models, it was assumed that the neutral and ionized fluids were fully coupled.

In the right-hand column of Fig. 3 are plotted the temperature profile, fractional abundance of H, n(H)/$n_{\rm H}$, and n(ortho)/n(para) for J-type shocks with a range of shock speeds, $10 <$ $V_{\rm s}$$<$ 25 km s^{-1}. As for the C-type shocks in Fig. 3, the initial gas density is $n_{\rm H}$= 10^4 cm^{-3}, and the initial ortho:para ratio is 0.01.

Table 3. Shock structure, H_2 ortho:para ratios, and $v = 0 - 0$ line fluxes (in erg cm^{-2} s^{-1} sr^{-1}) for $n_{\rm H}$= 10^4 cm^{-3}

C-shocks, $n_H = 10^4$ cm^{-3}, $B_0 = 100\mu G$																			
(o/p)$_{\rm init} = 0.01$																			
$V_{\rm s}$	L(cm)	t(yr)	n(H)/$n_{\rm H}$	$T_{\rm n}^{\rm max}$	$\langle T_J \rangle$	$\langle T_J \rangle_{\rm v=1}$	(o/p)$_{\rm max}$	$\frac{N(o)}{N(p)}$	$(o/p)_{\rm CAM}$	$(o/p)_{\rm v=1}$	$\varepsilon_{\rm H_2}$	$\varepsilon_{\rm CAM}$	S(0)	S(1)	S(2)	S(3)	S(4)	S(5)	S(6)	S(7)
10	1.7(17)	1.1(4)	3.8(-4)	231	146	175	0.01	0.01	0.01	0.01	18	1.5	2.6(-5)	7.3(-7)	1.6(-5)	3.6(-9)	1.4(-9)	…	…	…
20	1.2(17)	4.4(3)	9.8(-4)	781	357	524	0.28	0.23	0.13	0.10	50	47	6.9(-5)	1.6(-4)	2.5(-3)	3.2(-4)	6.9(-4)	9.6(-6)	4.8(-6)	1.6(-8)
30	1.2(17)	3.3(3)	1.8(-3)	1340	591	880	2.84	2.12	1.13	0.79	67	63	3.1(-5)	9.6(-4)	2.4(-3)	6.5(-3)	4.4(-3)	2.1(-3)	4.8(-4)	5.2(-5)
40	1.1(17)	2.4(3)	3.4(-3)	1970	835	1340	3.00	2.58	1.98	1.61	74	70	2.5(-5)	1.2(-3)	2.4(-3)	1.3(-2)	8.3(-3)	1.3(-2)	3.3(-3)	1.6(-3)
(o/p)$_{\rm init} = 1$																			
$V_{\rm s}$	L(cm)	t(yr)	n(H)/$n_{\rm H}$	$T_{\rm n}^{\rm max}$	$\langle T_J \rangle$	$\langle T_J \rangle_{\rm v=1}$	(o/p)$_{\rm max}$	$\frac{N(o)}{N(p)}$	$(o/p)_{\rm CAM}$	$(o/p)_{\rm v=1}$	$\varepsilon_{\rm H_2}$	$\varepsilon_{\rm CAM}$	S(0)	S(1)	S(2)	S(3)	S(4)	S(5)	S(6)	S(7)
10	1.7(17)	1.1(4)	3.8(-4)	226	145	173	1.00	1.00	0.98	0.80	6.0	0.8	1.3(-5)	3.5(-5)	7.4(-6)	1.5(-7)	…	…	…	…
20	1.3(17)	4.6(3)	9.8(-4)	776	358	525	1.32	1.26	1.22	1.16	50	42	3.7(-5)	5.7(-4)	1.3(-3)	1.4(-3)	3.6(-4)	5.0(-5)	2.4(-6)	9.0(-8)
30	1.1(17)	3.2(3)	1.8(-3)	1340	588	887	2.95	2.64	2.09	1.81	67	63	2.6(-5)	1.1(-3)	1.8(-3)	7.7(-3)	3.1(-3)	2.7(-3)	3.1(-4)	7.6(-5)
40	1.1(17)	2.4(3)	3.4(-3)	1970	828	1341	3.00	2.85	2.57	2.34	74	70	2.4(-5)	1.2(-3)	2.1(-3)	1.4(-2)	7.1(-3)	1.4(-2)	2.6(-3)	1.8(-3)
J-shocks, $n_H = 10^4$ cm^{-3}, $B_0 = 10\mu G$																			
(o/p)$_{\rm init} = 0.01$																			
$V_{\rm s}$	L(cm)	t(yr)	n(H)/$n_{\rm H}$	$T_{\rm n}^{\rm max}$	$\langle T_J \rangle$	$\langle T_J \rangle_{\rm v=1}$	(o/p)$_{\rm max}$	$\frac{N(o)}{N(p)}$	$(o/p)_{\rm CAM}$	$(o/p)_{\rm v=1}$	$\varepsilon_{\rm H_2}$	$\varepsilon_{\rm CAM}$	S(0)	S(1)	S(2)	S(3)	S(4)	S(5)	S(6)	S(7)
5	1.2(14)	1.1(2)	8.3(-4)	1230	509	674	0.04	0.04	0.02	0.02	31	31	4.8(-7)	2.0(-7)	1.7(-5)	6.8(-7)	1.7(-5)	1.3(-7)	1.0(-6)	2.1(-9)
10	4.1(13)	3.9(1)	1.2(-3)	5200	1342	2746	1.07	0.94	0.48	0.22	71	36	1.9(-7)	2.6(-6)	1.5(-5)	2.6(-5)	7.6(-5)	4.8(-5)	1.4(-4)	3.5(-5)
15	1.8(13)	1.8(1)	1.2(-2)	11800	1742	4480	3.00	2.87	2.42	1.63	80	13	6.2(-8)	3.0(-6)	5.1(-6)	3.9(-5)	2.9(-5)	1.1(-4)	6.8(-5)	1.7(-4)
20	1.1(13)	1.2(1)	1.2(-1)	21100	1776	4653	3.00	2.94	2.77	2.64	71	4.0	4.4(-8)	2.1(-6)	3.4(-6)	2.6(-5)	1.8(-5)	7.7(-5)	4.0(-5)	1.4(-4)
25	9.8(12)	8.7(0)	4.4(-1)	33000	2000	4822	3.00	2.93	2.81	2.78	45	1.6	2.4(-8)	1.2(-6)	2.1(-6)	1.7(-5)	1.2(-5)	5.7(-5)	3.1(-5)	1.2(-4)
(o/p)$_{\rm init} = 1$																			
$V_{\rm s}$	L(cm)	t(yr)	n(H)/$n_{\rm H}$	$T_{\rm n}^{\rm max}$	$\langle T_J \rangle$	$\langle T_J \rangle_{\rm v=1}$	(o/p)$_{\rm max}$	$\frac{N(o)}{N(p)}$	$(o/p)_{\rm CAM}$	$(o/p)_{\rm v=1}$	$\varepsilon_{\rm H_2}$	$\varepsilon_{\rm CAM}$	S(0)	S(1)	S(2)	S(3)	S(4)	S(5)	S(6)	S(7)
5	1.2(14)	1.1(2)	8.3(-4)	1230	523	682	1.04	1.04	1.01	1.02	32	30	2.4(-7)	2.9(-6)	8.8(-6)	1.3(-5)	8.9(-6)	3.2(-6)	5.7(-7)	5.8(-8)
10	4.0(13)	3.9(1)	1.2(-3)	5200	1411	2949	2.05	1.95	1.53	1.25	71	39	1.2(-7)	3.7(-6)	9.2(-6)	4.1(-5)	4.5(-5)	9.7(-5)	7.5(-5)	9.4(-5)
15	1.8(13)	1.8(1)	1.2(-2)	11800	1725	4421	3.00	2.96	2.79	2.38	81	14	6.1(-8)	3.0(-6)	4.9(-6)	3.9(-5)	2.7(-5)	1.2(-4)	5.8(-5)	1.8(-4)
20	1.1(13)	1.2(1)	1.2(-1)	21100	1770	4623	3.00	2.98	2.92	2.87	71	4.1	4.4(-8)	2.1(-6)	3.4(-6)	2.7(-5)	1.7(-5)	7.9(-5)	3.8(-5)	1.4(-4)
25	9.8(12)	8.7(0)	4.4(-1)	33000	1995	4806	3.00	2.98	2.93	2.93	45	1.6	2.4(-8)	1.2(-6)	2.0(-6)	1.7(-5)	1.2(-5)	5.8(-5)	3.0(-5)	1.2(-4)

Column contents: $V_{\rm s}$ is the shock speed (in km s^{-1}); L is the width of the region in which $T_{\rm n}>$ 50 K; t is the time required for the neutral fluid to traverse the width of the shock wave; n(H)/$n_{\rm H}$ is the maximum H abundance in the shock wave; $T_{\rm n}^{\rm max}$ is the maximum temperature of the neutrals; $\langle T_J \rangle$ is the mean of the excitation temperature T_J for levels $v = 0, J = 5$ to 8; $\langle T_J \rangle_{\rm v=1}$ is the mean of the excitation temperature T_J for levels $v = 1, J = 1$ to 11; (o/p)$_{\rm max}$ is n(ortho)/n(para), and $\frac{N(o)}{N(p)}$ is N(ortho)/N(para), evaluated at the rear of the shock wave (where $T_{\rm n}$ has fallen to 50 K); $(o/p)_{\rm CAM}$ is the mean of the empirical ortho:para ratio, derived for levels $v = 0, J = 5$ to 8; $(o/p)_{\rm v=1}$ is the mean of the empirical ortho:para ratio, derived for levels $v = 1, J = 1$ to 11; $\varepsilon_{\rm H_2}$ is the percentage of the initial mechanical energy flux ($\rho V_s^3/2$) radiated in all the lines of H_2 included in the model; $\varepsilon_{\rm CAM}$ is the percentage of the initial mechanical energy flux radiated in the transitions 0-0 S(2) to S(7); S(J) is the flux radiated in the H_2 0-0 S(J) line in a direction perpendicular to the shock surface, in erg cm^{-2} s^{-1} sr^{-1} (values below 10^{-9} are replaced by …). In all columns, parentheses indicate powers of ten.

Both C- and J-type shocks involve an initial rise in the temperature, followed by radiative cooling and compression of the gas towards its postshock state. However, the quasi-discontinuous temperature rise associated with a J-type shock ensures that the maximum temperature is attained adiabatically, and it is consequently much higher than in a C-type shock of the same speed. Thus, whilst a C-type shock with V_s= 20 km s^{-1} gives rise to a maximum temperature T_n^{max}= 800 K of the neutral gas (see Fig. 3a), T_n^{max}= 2×10^4 K in the corresponding J-type shock (Fig. 3e).

The high maximum temperatures in J-type shocks give rise to much more rapid radiative cooling, by rovibrational transitions of molecular hydrogen, than in the corresponding C-type shocks. Thus, the width of a J-type shock with V_s= 20 km s^{-1} and initial n_H= 10^4 cm^{-3} is of the order of 10^{13} cm, as compared with 10^{17} cm for a C-type shock of the same speed. The corresponding times of flow through the shocks are 13 yr and 4000 yr, respectively. Evidently, H_2 emission lines of high excitation energy are much more intense, relative to those of low excitation energy, under J-type shock conditions.

The treatment of radiative cooling is crucial when determining the structure of and H_2 line emission from the postshock flow. Chang & Martin (1991) made predictions of H_2 line intensities in J-type shocks, considering H_2 cooling only. With the same parameters as in their model 10k5 (n_H= 2×10^5 cm^{-3}, T_n^{max}= 10^4 K, V_s= 15 km s^{-1}), and with B = 45 μG, we find that H_2 cooling dominates down to about only 1000 K. The approximation of neglecting coolants other than H_2 is, therefore, inadequate when the preshock gas density is so high. We have also compared our results for n_H= 10^4 cm^{-3} and V_s= 10 km s^{-1} with those of Burton et al. (1992) obtained with the J-type shock code of Hollenbach & McKee (1989). We find good agreement (within 10%) for the 0-0 S(1) to S(3) lines but predict 3 times more flux in the 1-0 S(1) line. The intensities of the pure rotational lines agree because the populations of the low rotational levels are close to thermal equilibrium.

3.2.2. Dissociation of H_2 and para to ortho conversion

The process of para to ortho conversion is more rapid in J- than in C-type shocks, owing to the higher postshock temperatures. However, the time available for conversion is much shorter, typically by a factor of 100, owing to the rapid cooling in the dense postshock flow. As a result, we find that para to ortho conversion does not occur for V_s= 5 km s^{-1}(T_n^{max}= 1000 K) and that it remains incomplete in J-shocks where the maximum temperature is below 10^4 K, i.e. $V_s \leq$ 10 km s^{-1}(Fig. 3g).

When the postshock temperature exceeds 10^4 K, the rate coefficients for dissociation of H_2 in H and H_2 collisions become sufficiently large for these processes to dominate the dissociation of molecular hydrogen (Fig. 3h). Indeed, for n_H= 10^4 cm^{-3} and V_s= 25 km s^{-1}, n(H)/$n_H \approx$ 0.4 in the postshock gas (Fig. 3f). The high abundance of atomic H then ensures that conversion of para- to ortho-H_2 proceeds rapidly and that the statistical value of 3 is attained. Similar results were obtained for the other values of n_H that we investigated, with complete conversion requiring $T_n^{max} > 10^4$ K, i.e. $V_s \geq$ 15 km s^{-1}.

3.2.3. Electronic tables

We provide in Table 4a-f (electronic form only, available at `CDS` and from `http://ccp7.dur.ac.uk/`) an extensive set of parameters, derived from our grid of J-type shock models, in the same format as Tables 2a-f for C-type shocks. By way of illustration, Table 3 contains a subset of Table 4a-b, for n_H= 10^4 cm^{-3} and (o/p)$_{init}$ = 0.01 and 1.

4. Comparison with observations and diagnostic diagrams

4.1. Observed value of the ortho:para ratio

The ortho:para ratio, n(ortho)/n(para), plotted in Fig. 3c and Fig. 3g, is the local value at each position in a planar C- or J-type shock wave. An observer, on the other hand, measures H_2 populations integrated over the shock width and, as we shall now see, deduces an ortho:para ratio which is always lower than the final value, reached behind the shock wave.

The method by which the ortho:para ratio is determined observationally is illustrated in Fig. 4a. This method makes use of the excitation diagram, which is a plot of $\ln[N_J/g_J g_I]$ against E_J/k_B, where N_J is the column density measured in rotational level J, and E_J is the excitation energy of this level, relative to $J = 0$; $g_J = 2J + 1$ and $g_I = 1$ (J even) or 3 (J odd). If the rotational sublevels are populated according to a Boltzmann distribution at temperature T_{rot}, and if the ortho:para ratio is equal to its LTE value at T_{rot}, then

$$\mathrm{ortho:para(LTE},T_{rot}) = \frac{\sum\limits_{Jodd} 3(2J+1)e^{-E_J/(k_B T_{rot})}}{\sum\limits_{Jeven} (2J+1)e^{-E_J/(k_B T_{rot})}} \quad (4)$$

and the excitation diagram is a straight line of slope $-1/T_{rot}$. The downwards displacement of the line joining points corresponding to odd J (ortho-H_2), relative to even J (para-H_2), provides a measure of the departure of the ortho:para ratio from its value in thermal equilibrium at T_{rot}. For each ortho level J, the ortho:para ratio is obtained from

$$\frac{\mathrm{ortho:para(J)}}{\mathrm{ortho:para(LTE,T_J)}} = \frac{N_J}{N_J(\mathrm{LTE},T_J)}, \quad (5)$$

where the excitation temperature between levels $J+1$ and $J-1$, T_J, is given by

$$T_J = \frac{E_{J+1} - E_{J-1}}{k_B \ln(N_{J-1} g_{J+1}/N_{J+1} g_{J-1})} \quad (6)$$

and $N_J(\mathrm{LTE},T_J)$ is the column density obtained by linear interpolation between the points $J-1$ and $J+1$ in the excitation diagram (see Fig. 4a). In practice, the excitation diagram may exhibit curvature, indicative of the emitting gas having a range of kinetic temperatures. The curvature is small for C-type and greater for J-type shocks, owing to the very rapid variation of the kinetic temperature in the post J-shock flow. Curvature can

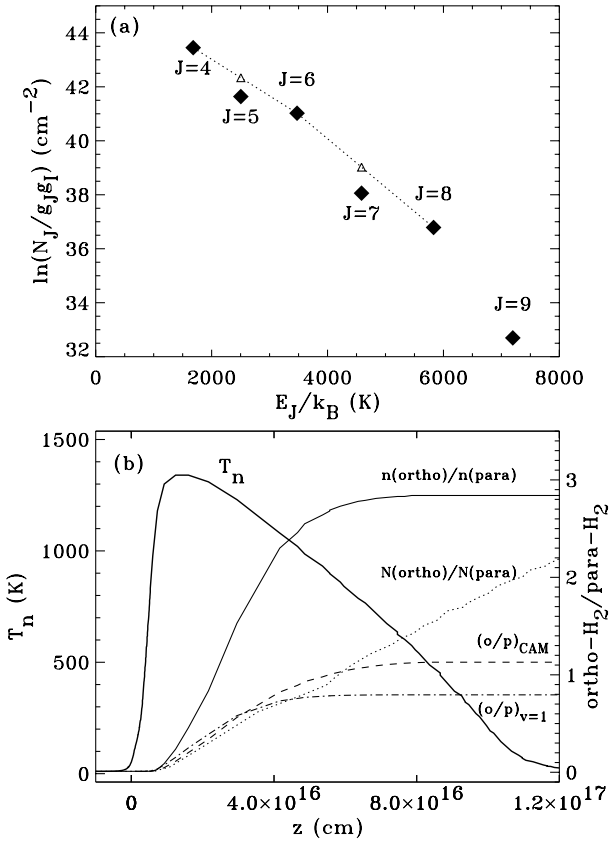

Fig. 4. a An excitation diagram, obtained using the column densities of the rotational levels $4 \leq J \leq 9$ from a model of a C-type shock in which V_s= 30 km s^{-1} and, initially, n_H= 10^4 cm^{-3} and ortho:para = 0.01; triangles show the LTE populations $N_J(\mathrm{LTE}, T_J)$ used to estimate the ortho:para ratio (see text, Sect. 4.1, Eq. (5)). **b** The local ortho:para density ratio, n(ortho-H_2)/n(para-H_2), and the ratio of the corresponding column densities, N(ortho-H_2)/N(para-H_2), plotted as functions of distance through a model of a C-type shock in which V_s= 30 km s^{-1} and, initially, n_H= 10^4 cm^{-3} and ortho:para = 0.01. Also plotted in this figure are the values of the ortho:para ratio derived, as described in Sect. 4.1, from the column densities of the rotational levels v = 0, J = 5 to J = 8 [$(o/p)_{\mathrm{CAM}}$] and v = 1, J = 1 to J = 11 [$(o/p)_{\mathrm{v=1}}$].

introduce systematic errors in the ortho:para ratio determined from Eq. (5), but we find that averaging over an equal number of ortho and para levels yields a reliable value (with error $\leq$ 20%).

It is important to realize that the ortho:para ratio derived empirically depends on the lines that are observed: levels with differing excitation energies are populated in different parts of the shock wave, where the (local) values of the ortho:para ratio may also differ. To illustrate this important point, we plot in Fig. 4b the variations of measures of the ortho:para ratio through a C-type shock wave in which V_s= 30 km s^{-1} and, initially, n_H= 10^4 cm^{-3} and ortho:para = 0.01. In this model, the local ortho:para ratio, n(ortho)/n(para), reaches its final (and maximum) value of 2.85 at a distance $z \approx 7 \times 10^{16}$ cm (flow time $t \approx 2000$ yr); the shock pulse is delineated by the neutral temperature profile. The ratio of total column densities in the ortho- and para-H_2 levels, N(ortho)/N(para), integrated up to the current point in the profile, is seen to lag behind the local ortho:para ratio, attaining its final (maximum) value only for sufficiently long integration times after the shock pulse. This ratio is difficult to determine observationally, as most of the cool postshock H_2 lies in the J = 0 and J = 1 levels, the populations of which are measurable only in absorption; foreground and background cold molecular material add further, unknown contributions to the column densities of these levels.

In emission line studies, the column densities of levels with $J \geq 2$ are measured, and the inferred ortho:para ratio differs from N(ortho)/N(para). Additionally plotted in Fig. 4b is $(o/p)_{\mathrm{CAM}}$, the mean value of the empirical ortho:para ratios derived from Eq. (5-6) for levels $v = 0, 5 \leq J \leq 8$ (using e.g. the H_2 0-0 S(2) to S(7) lines falling in the ISOCAM spectral range), integrated up to the current point in the profile. This ratio first follows closely the total column density ratio, N(ortho)/N(para) but attains a limiting value when the gas has cooled to about 500 K. The levels considered, which have $E_J >$ 1600 K, are not significantly populated at low temperatures, and their integrated column densities become effectively "frozen". As a consequence, this empirical ratio does not depend on the (unknown) amount of cool preshock and postshock gas along the line of sight, enabling a meaningful comparison to be made between ISOCAM observations and the shock models.

Finally, Fig. 4b also plots $(o/p)_{\mathrm{v=1}}$, the mean value of the ortho:para ratios empirically derived from column densities of the levels $v = 1, 1 \leq J \leq 11$ (corresponding to the upper levels of the ro-vibrational $v = 1 - 0$ lines observable from the ground). These levels have higher energies (6000 to 14000 K) than the $v = 0, 5 \leq J \leq 8$ levels; thus, the column density ratios become "frozen" even sooner after the temperature maximum, and $(o/p)_{\mathrm{v=1}}$ remains smaller than $(o/p)_{\mathrm{CAM}}$. We conclude that an object where $(o/p)_{\mathrm{v=1}} > (o/p)_{\mathrm{CAM}}$ cannot be explained by the presence of a single stationary-state planar shock wave within the observing beam.

4.2. Diagnostic diagrams and application to HH 54

4.2.1. Pure rotational lines in C-type shocks

Neufeld et al. (1998) have used ISO SWS02 (grating mode) observations of the E,K emission knots in HH 54, together with the C-shock models of Timmermann (1998), to constrain the shock speed and preshock ortho:para ratio in this object. They have shown that a useful diagnostic diagram is obtained by plotting the line intensity ratio S(3)/S(1) (a measure of the excitation temperature T_J) as a function of S(2)/S(1) (a measure of both T_J and the ortho:para ratio) for a range of shock models with fixed preshock density. With an arbitrarily chosen n_H = 10^6 cm^{-3}, the corresponding observational point indicates a shock speed of 22 km s^{-1} and an initial ortho:para ratio of $\leq$ 0.2, accepting some extrapolation of Timmermann's results below $(o/p)_{\mathrm{init}}$ = 1.

In view of the improvements that we have made, in the treatment of H_2 excitation, for example, and of the discrepancies with the results of Timmermann (1998), we present in this section

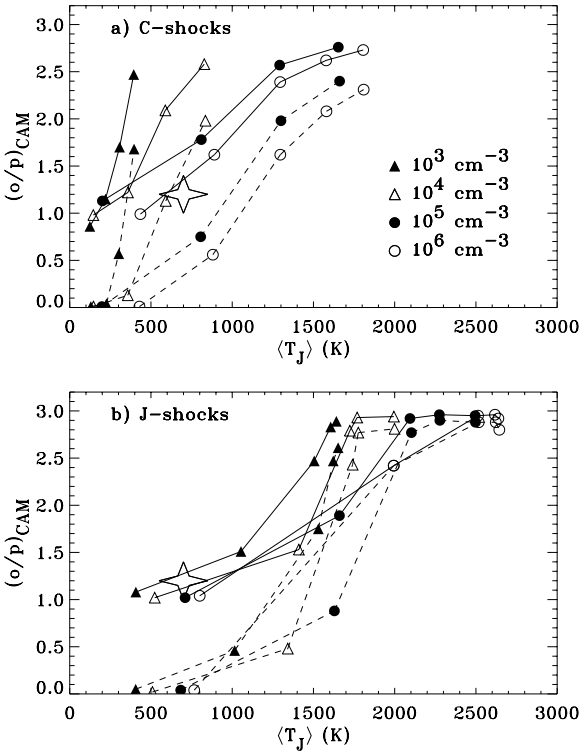

Fig. 5a and b. The mean observed ortho:para ratio, derived from levels $v = 0, J = 5$ to 8, plotted against the mean excitation temperature of these same levels, for a range of shock speeds, preshock densities, and initial ortho:para ratios (see text, Sect. 4.2): **a** C-type shocks; **b** J-type shocks. Solid curves correspond to $(o/p)_{\rm init}$ = 1.0, dashed curves to $(o/p)_{\rm init}$ = 0.01; each point on a given curve represents a different shock speed. The point plotted as a star derives from SWS02 observations of HH 54 E,K (Neufeld et al. 1998).

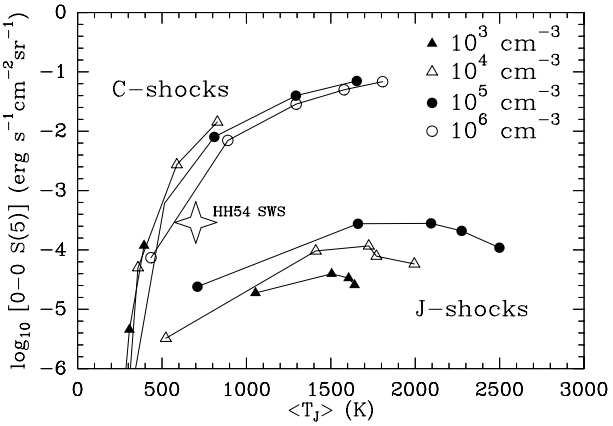

Fig. 6. The computed intensity of the 0-0 S(5) line, plotted against the mean excitation temperature, for a range of C- and J-type shock models with an initial ortho:para ratio of 1 (see text, Sect. 4.2). The point plotted as a star derives from SWS02 observations of HH 54 E,K (Neufeld et al. 1998).

diagnostic diagrams which derive from our own grid of models and which cover a wider range in $(o/p)_{\rm init}$ and $n_{\rm H}$. Our diagnostic diagram is analogous to that in Neufeld et al. (1998), but we focus on the levels emitting lines in the ISOCAM range ($0-0$ S(2) to S(7)). Along the x-axis, we plot $\langle T_J \rangle$, the mean value of the excitation temperature, T_J, defined by Eq. (6) above and deduced for $v = 0$, J = 5, 6, 7 and 8 from the ISOCAM lines. Along the y-axis, we plot $(o/p)_{\rm CAM}$, the corresponding mean value of the ortho:para ratios, deduced for these same levels using Eq. (5).

Fig. 5a is such a diagnostic diagram, for $n_{\rm H}$= 10^3, 10^4, 10^5, and 10^6 cm^{-3}. Solid curves correspond to an initial ortho:para ratio of 1.0, dashed curves to 0.01; an initial ortho:para ratio $<$ 0.01 yields the same results as 0.01. Each point on a given curve represents a different shock speed. As the shock speed (and temperature) increases, reactions of H with H_2 begin to occur, and the ortho:para ratio deduced from the ISOCAM lines rises, reaching values in excess of 2.0 for $V_s = 40$ km s^{-1}. Being an average over the shock thickness, the ortho:para ratio never attains 3.0 (see Sect. 4.1).

Fig. 5a shows that the rise in the ortho:para ratio occurs at lower excitation temperatures as $n_{\rm H}$ decreases. This shift of the diagnostic curves with $n_{\rm H}$ has two important consequences. First, any given observed point, when plotted in this diagram, does not correspond to unique values of both the initial ortho:para ratio and $V_{\rm s}$. Adopting a lower $n_{\rm H}$ yields a lower initial ortho:para ratio and a higher $V_{\rm s}$; this introduces an intrinsic uncertainty in the determination of the preshock parameters. Second, the curve corresponding to a very low initial ortho:para ratio (0.01 in Fig. 5a) defines for each $n_{\rm H}$ the minimum ortho:para ratio at a given excitation temperature. An observed point located below this curve is incompatible with the models at the corresponding value of $n_{\rm H}$ and implies a higher preshock density.

As an illustration, we plot as a star symbol in Fig. 5a the point which derives from the SWS observations of HH 54 (Neufeld et al. 1998). We see that values of $n_{\rm H} < 10^4$ cm^{-3} are excluded by this observation. For $n_{\rm H}$= 10^4, 10^5, and 10^6 cm^{-3}, the inferred pairs of values of $V_{\rm s}$ and $(o/p)_{\rm init}$ are, respectively, (30 km s^{-1}, ≤ 0.01), (20 km s^{-1}, 0.5), and (15 km s^{-1}, 0.8). In order to determine the initial ortho:para ratio, we require an independent constraint on $n_{\rm H}$ but the observed H_2 line fluxes are not sufficient for this purpose. As Fig. 6 shows, for a given excitation temperature and value of $(o/p)_{\rm init}$ (= 1.0 in Fig. 6), the intensity of the 0-0 S(5) line differs by at most a factor of 3 among C-shock models with $n_{\rm H}$ ranging from 10^3 to 10^6 cm^{-3}. This weak dependence on $n_{\rm H}$ stems from the inverse proportionality of the shock thickness to $n_{\rm H}$, which results in an almost invariant total H_2 column density through the shock wave (1.5×10^{21} cm^{-2}, to within 50%). Additional uncertainties in the filling factor of the shock layer in the instrument beam make it difficult to constrain $n_{\rm H}$ from line fluxes alone. The shock thickness might provide a more stringent constraint (cf. Table 2a). In HH 54, high $n_{\rm H}$ values would be favored if the rotational emission arises from small knots of $\sim 5''$ (1.5×10^{16} cm), as observed in rovibrational lines. However, ISOCAM images suggest that the H_2 emission is more widespread (Cabrit et al. 1999).

We conclude that the initial ortho:para ratio $(o/p)_{\rm init} < 0.8$ in the region of HH 54 observed by SWS but that the uncertainties

in $n_{\rm H}$ are such that it is not possible to decide whether the ratio has reached thermal equilibrium in the preshock gas.

4.2.2. Pure rotational lines in J-type shocks

Fig. 5b is the diagnostic diagram for our grid of J-type shock models with $n_{\rm H}$ = 10^3, 10^4, and 10^5 cm^{-3}. The results are broadly similar to those for C-type shocks, but the rise in the ortho:para ratio occurs at much higher excitation temperatures, $>$ 1000 K. The shifts between curves corresponding to different values of $n_{\rm H}$ are smaller than in the case of C-type shocks. It follows that the inferred values of the initial ortho:para ratio and shock speed are less sensitive to the assumed $n_{\rm H}$. From the observations of HH 54 by Neufeld et al. (1998), we deduce (o/p)$_{\rm init}$ $\approx$ 1.0 and $V_{\rm s}\approx$ 5 km s^{-1}.

In Fig. 6 are plotted the fluxes in the 0-0 S(5) line, as a function of the excitation temperature, for our J-type shock models. The line flux is slightly more sensitive to $n_{\rm H}$ than is the case for C-type shocks. However, the predicted line fluxes for J-type shocks are at least an order of magnitude below the flux observed in HH 54 by ISO SWS. A J-type shock could account for the observed flux only if the preshock gas is dense ($n_{\rm H}$= 10^5 cm^{-3}) and the shock front is curved over a scale comparable to the beam size.

4.2.3. Rovibrational transitions as diagnostics

Prior to the launch of ISO, H_2 emission lines from shocks driven by young stellar objects were observable only from the ground by means of the $v = 1-0$ transitions in the H and K atmospheric bands. Relative populations in the $v = 1$ levels were used to deduce a mean rotational excitation temperature, typically in the range 2000-3000 K, and a mean ortho:para ratio in the range 2.5 to 3.0 (e.g. Gredel 1994; Smith et al. 1997).

In principle, such observations may also be used to constrain the initial ortho:para ratio in the pre-shock gas. We present in Fig. 7 diagnostic diagrams equivalent to those in Fig. 5, but for the $v = 1$ levels of H_2. We plot along the x-axis $\langle T_J\rangle_{\rm v=1}$, the mean value of the excitation temperature T_J of the $v = 1, 1 \leq J \leq 11$ levels, and along the y-axis $(o/p)_{\rm v=1}$, the corresponding mean value of the ortho:para ratio, deduced for the same levels, as described in Sect. 4.1. The symbols and curves are the same as in Fig. 5.

Once again, we use the knots E,K in HH 54 as an illustration. The dashed rectangle in Fig. 7 indicates the range of parameters compatible with near infrared observations of these emission knots by Gredel (1994). We first note that $(o/p)_{\rm v=1}$ is larger than $(o/p)_{\rm CAM}$, which suggests that a single planar shock wave within the SWS beam cannot account for all of the observations (cf. Sect. 4.1). Indeed, the rotational excitation temperature in $v = 1$, $\langle T_J\rangle_{\rm v=1}\approx$ 2900 K, implies a faster C-type shock ($V_{\rm s}>$ 35 km s^{-1}) than the pure rotational transitions observed from HH 54. The corresponding initial ortho:para ratio is ill-determined. At such high shock speeds, para to ortho conversion is fast enough to yield an observed ratio close to 3.0, regardless of the initial value. In the case of a J-type shock, we

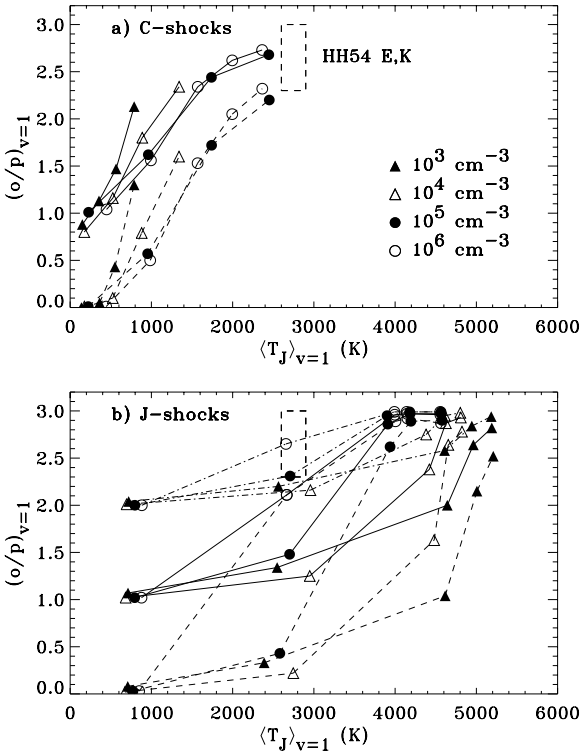

Fig. 7a and b. The mean observed ortho:para ratio in levels $v = 1, J =$ 1 to 11, plotted against the mean excitation temperature of these same levels, for a range of shock speeds, preshock densities, and initial ortho:para ratios (see text, Sect. 4.2.3): **a** C-type shocks; **b** J-type shocks. The dashed rectangle derives from H- and K-band spectroscopic observations of HH 54 E,K (Gredel 1994).

infer $V_{\rm s}$= 10 km s^{-1} and a better constrained initial ortho:para ratio $\geq$ 2.0, higher than deduced from the pure rotational lines ($\leq$ 1.0 for both C-type and J-type shocks).

The situation that vibrational transitions imply a higher shock speed than pure rotational transitions is also found in other protostellar outflows observed with ISO (e.g. Cep A; Wright et al. 1996). Similar difficulties were already encountered when trying to reconcile all H_2 lines observed across the near-IR range with a single planar shock (e.g. Smith & Brand 1990). A solution proposed by previous authors (e.g. Smith et al. 1991) is that the shock front is curved within the beam (bow shock): rovibrational emission probes regions closer to the bow apex, where the shock speed is higher, while pure rotational lines probe further out in the bow shock wings. The curved front could be entirely of one (C- or J-) type or contain both C-type and J-type surfaces. Studies of the ortho:para ratio using both sets of lines could impose additional constraints on this model. In the case of HH 54 E,K, the initial ortho:para ratio $\geq$ 2.0 deduced from the vibrational transitions, assuming a J-type shock, is incompatible with the value $\leq$ 1 from the pure rotational lines. A C-type bow shock with an initial ortho:para ratio $<$ 0.8 and $V_{\rm s} >$ 35 km s^{-1} remains a possibility.

An alternative explanation of the rotational and vibrational line emission is that the shock wave has not reached steady-state (Chièze et al. 1998). In this model, the rotational lines arise

mainly in the C-type component, whilst the vibrational lines come from the following J-type component (Flower & Pineau des Forêts 1999). The initial ortho:para ratio, ahead of the shock wave, could be low (< 0.8), as required by the pure rotational lines, but the ratio could increase in the magnetic precursor to a local value of 2.0 just ahead of the J-discontinuity, as required by the vibrational lines. A more detailed investigation of these possibilities in relation to HH 54 and other objects is deferred to a subsequent paper.

5. Concluding remarks

– We have investigated the process of para to ortho conversion, driven by H-H_2 nuclear spin-changing reactions, in stationary shocks of both C- and J-type, paying particular attention to the chemistry, ion-neutral coupling within the shock wave, and collision-induced transitions in H_2.
– Chemical conversion of oxygen into water is the main source of atomic H in C-type shocks with $V_s \leq 20$ km s^{-1}. At higher shock speeds, dissociation by ion impact further increases the atomic fraction, but by no more than a factor of about 3. In J-type shocks, chemical dissociation dominates for $V_s \leq$ 10 km s^{-1}; at higher speeds, collisional dissociation by H and H_2 becomes effective, increasing the atomic fraction by orders of magnitudes over the chemical value.
– Over a wide range of densities and velocities, the degree of para to ortho conversion is found to be determined mainly by the maximum temperature attained by the neutrals in the shock, T_n^{max}. In C-type shocks, where the flow time is long, significant conversion starts at $T_n^{max} \approx 700$ K and is complete for $T_n^{max} \geq 1300$ K, even though the fraction of atomic hydrogen remains low. In J-type shocks, where the time available for conversion is much less, the ortho:para ratio starts to increase only for $T_n^{max} > 1000$ K. Complete conversion requires n(H)/$n_H \geq 10^{-2}$, which occurs in our models for $T_n^{max} \geq 10^4$ K, i.e. for $V_s \geq 15$ km s^{-1}.
– Our results for C-type shocks differ significantly from those of Timmermann (1998). We find much lower abundances of H^+ and H_3^+ and a much lower fraction of atomic H, even when we adopt his (larger) rate coefficient for dissociation of H_2 by ion impact. The net effect is that Timmermann's calculations overestimate the final ortho:para ratio.
– The ortho:para ratio deduced from observations of levels above $v = 0, J = 2$ is always lower than the ratio of the total ortho-H_2 and para-H_2 column densities through the shock wave, which is itself lower than the maximum local value of the ortho:para ratio reached in the postshock gas. In addition, the observed ortho:para ratio depends on the lines that are used. For the same object, the pure rotational lines observed with ISOCAM should yield a higher ortho:para ratio than $v = 1 - 0$ rovibrational lines.
– We have examined constraints on the initial ortho:para ratio and shock speeds that can be derived from the observed H_2 excitation temperatures and ortho:para ratio, using both pure rotational lines and rovibrational lines. For C-type shocks, there may be a strong dependence on the assumed n_H. Adopting a lower n_H yields a lower initial ortho:para ratio and a higher V_s. For J-type shocks, the H_2 excitation temperatures typically observed in protostellar outflows correspond to low velocity shocks ($V_s \leq 10$ km s^{-1}) in which the observed ortho:para ratio is still close to its initial value, which is then better constrained.
– As an illustration, we have considered observations of H_2 in the knots E,K of the Herbig-Haro object HH 54 (Neufeld et al. 1998; Gredel 1994). The pure rotational lines imply an initial ortho:para ratio ≤ 1.0. In the case of a C-type shock with $n_H = 10^4$ cm^{-3}, the initial ratio could be as low as 0.01 (the LTE value at 25 K). As is often the case in protostellar flows, the rovibrational lines require the presence of a hotter component within the observing beam, distinct from that producing the pure rotational lines. The need for a distinct component arises independently in order to account for the higher ortho:para H_2 ratio deduced empirically from the rovibrational lines, as compared to the pure rotational lines. Assuming a uniform initial ortho:para ratio in the preshock gas, we show that either a C-type bow shock or a shock wave which has not reached steady-state (and possesses both C- and J-type characteristics) is a plausible model. Observations of the ortho:para H_2 ratio in various sets of lines seem to provide a useful way of determining the shock structures in protostellar outflows.

Acknowledgements. We are grateful to the Royal Society and the CNRS for financial support under the European Science Exchange Programme. One of the authors (DRF) gratefully acknowledges the award of a research fellowship by the University of Durham. We also thank the anonymous referee for his useful comments.

References

Breshears W.D., Bird P.F., 1973, 14th International Symposium on Combustion, The Combustion Institute, p. 211
Burton M.G., Hollenbach D.J., Tielens A.G.G.M., 1992, ApJ 399, 563
Cabrit S., Bontemps S., Lagage P.O., Sauvage M., Boulanger F., André P., Nordh L., Olofsson G., Cesarsky C.J., de Boula O., Sibille F., Siebenmorgen R. 1999, In: Cox P., Kessler M.F., (eds.) The Universe as seen by the Infrared Space Observatory (ISO). ESA, p. 449
Clavel J., Viala Y.P., Bel N., 1978, A&A 65, 435
Chang C.A., Martin P.G., 1991, ApJ 378, 202
Chièze J.-P., Pineau des Forêts G., Flower D.R., 1998, MNRAS 295, 672
Dalgarno A., Black J.H., Weisheit J.C., 1973, Astrophys. Lett. 14, 77
DeCampli W.M., Cameron A.G.W., Bodenheimer P., Black D.C., 1978, ApJ 223, 854
Devine D., Bally J., Reipurth B., Heathcote S., 1997, AJ 114, 2095
Dove J.E., Mandy M.E., 1986, ApJ 311, L93
Draine B.T., 1980, ApJ 241, 1021
Draine B.T., Roberge W.G., Dalgarno A., 1983, ApJ 264, 485
Flower D.R., Pineau des Forêts G., Field D., May P.W., 1996, MNRAS 280, 447
Flower D.R., Pineau des Forêts G., 1999, MNRAS 308, 271
Flower D.R., Watt G.D., 1984, MNRAS 209, 25
Gerlich D., 1990, J. Chem. Phys. 92, 2377
Gredel R., 1994, A&A 292, 580

Hollenbach D.J., McKee C.F., 1989, ApJ 342, 306
Jacobs T.A., Giedt R.R., Cohen N., 1967, J. Chem. Phys. 47, 54
Le Bourlot J., Pineau des Forêts G., Flower D.R., 1999, MNRAS 305, 802
Mathis H.S., Rumpl W., Nordsieck K.H., 1977, ApJ 217, 425
Neufeld D.A., Melnick G.J., Harwit M., 1998, ApJ 506, L75
Osterbrock D.E., 1962, ApJ 136, 359
Pineau des Forêts G., Flower D.R., McCarroll R., 1991, MNRAS 248, 173
Pineau des Forêts G., Flower D.R., Chièze J.-P., 1997, In: Reipurth B., Bertout C. (eds.) Herbig-Haro Flows and the Birth of Low-Mass Stars. Kluwer, Dordrecht, p. 199
Schilke P., Walmsley C.M., Pineau des Forêts G., Flower D.R., 1997, A&A 321, 293
Siegbahn P., Liu B., 1978, J. Chem. Phys. 68, 2457
Smith M.D., Brand P.W.J.L., 1990, MNRAS 243, 498
Smith M.D., Brand P.W.J.L, Moorhouse A., 1991, MNRAS 248, 451
Smith M.D., David C.J., Lioure A., 1997, A&A 327, 1206
Stibbe D.T., Tennyson J., 1998, New J. Phys. 1, 2.1
Timmermann R., 1998, ApJ 498, 246
Wright C.M., Drapatz S., Timmermann R., et al., 1996, A&A 315, L301